Visions and Strategies for Reinforcing Additively Manufactured Constructions 2025

Contribution to the symposium

https://doi.org/10.52825/ocp.v7i.2777

Published: 12 Dec. 2025

Robotic Fibre Winding Reinforcement

Fundamental Structural Engineering Principles

Bartłomiej Sawicki[1,*], Norman Hack[1], and Harald Kloft[1]

[1]Institute of Structural Design (ITE), TU Braunschweig, Germany

*Correspondence: Bartłomiej Sawicki, b.sawicki@tu-braunschweig.de

Abstract. The Digital Fabrication with Concrete (DFC) enables freedom of form. In order to fully leverage this freedom, the reinforcement should be rethought, as well. Such an opportunity is provided by the Robotic Fibre Winding (RFW). This in-situ and on-demand produced fibre reinforced polymer reinforcement can provide endless strands, which can be either digitally deposited on concrete (concrete defines the form) or on a frame with subsequent application of concrete (reinforcement defines the form), and combined particularly successful with the digital shotcrete or Shotcrete 3D Printing (SC3DP).

The current paper critically analyses the results of the three previously published experimental campaigns with glass fibre wound reinforcement: 1) one set of pull-out and direct tensile tests with various RFW reinforcement types embedded in cast concrete, and 2) two sets of four-point bending tests with two different RFW reinforcement types. In all cases the experimental results are re-analysed from the structural engineering point of view, with the special consideration of anchorage length required for the full activation of reinforcement.

On basis of the obtained results it is concluded, that despite theoretically good bond, resulting in required anchorage comparable to this of classical steel bars, many bending tests unexpectedly ended in pull-out failure. Hence, the mode of pull-out failure should be carefully observed in the upcoming experiments. Likewise, the focus should be put in the future on collection of all relevant data required for such detailed investigation of the bonding zone.

Keywords: GFRP, Testing, Analysis, Anchorage Length

1. Introduction

The digital fabrication with concrete (DFC) calls for new methods of reinforcement fabrication and integration. With digitally controlled concrete deposition tailored to form and function, the reinforcement should be able to do likewise. This is enabled by in-situ on-demand fabricated Fibre Reinforcement Polymer (FRP) reinforcement as enabled by the dynamic winding process [1].

The winding process takes place in a purposefully designed Dynamic Winding Machine (DWM) able to deliver endless reinforcement strands. The continuous process provides a range of reinforcement types depending on the raw material and fabrication parameters, such as: 1) mass diameter (tex) of primary yarn; and 2) tex, winding density, and pretension of the secondary yarn helically wound around the primary one [1], [2]. Thanks to the in-situ fabrication, the reinforcement strand can be deposited before the impregnating resin hardens. This enables novel construction processes where force-flow guided reinforcement is interacting with

concrete to define a unique structural form [3], such as: 1) robotic frame winding with subsequent deposition of concrete on reinforcement (reinforcement supports concrete) [4]; 2) winding on the concrete core with subsequent deposition of concrete cover (concrete supports reinforcement) [5], or 3) winding of reinforcement with subsequent embedment in concrete (no mutual support between concrete and reinforcement) [6].

The current paper aims to critically re-analyse available experimental testing results of dynamically wound E-Glass Fibre Reinforced Polymer (GFRP) reinforcement, with the special consideration of tensile and concrete bond strengths. Their relation is critical from the structural engineering point of view, and reflected in the minimum anchorage length required for the full activation of reinforcement. This indicator defines the scale of experimental specimens, but even more importantly the detailing of structural elements, and therefore sets the boundary condition for the freedom of form. Since it is defined by interrelation of the fabrication method details, parameters, and quality, the knowledge on mass-produced GFRP reinforcement bars is of no relevance here. To this end, direct tensile and pull-out testing [2] is analysed to define the anchorage length, while the result of four point bending of reinforced plates [4], [7] and principles of inverse analysis [8] are used in order to verify those values in the scale closer to the structural.

2. Direct pull-out testing

The results of direct tensile and pull-out testing, presented in [2], are re-analysed. A set of specimens was prepared and tested according to RILEM recommendations [9], see Figure 1. The reinforcement was embedded in cast concrete (Nafufill KM 250, max. aggregate 2 mm) cube with an edge length of 200 mm. Using a plastic tube protected with silicone for debonding, the bond length was set to $l_b = 5 \cdot d_b$. The tests were executed under displacement control with constant displacement rate of 0.02mm/s.

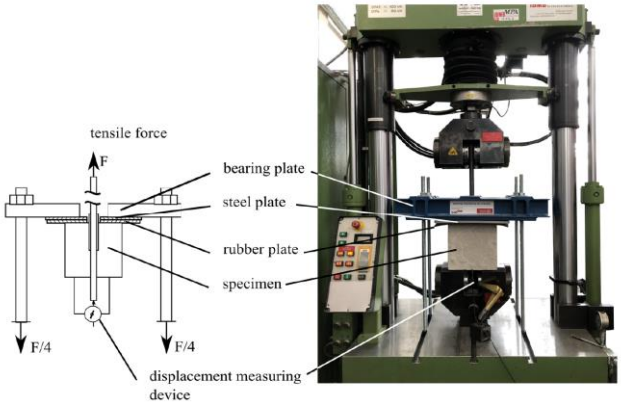

Figure 1. *Scheme and photograph of testing setup for direct pull-out of reinforcement from concrete cube adapted from [2]*

2.1 Theoretical required anchorage length

The minimum required anchorage length allows for the full activation of reinforcement, i.e., achieving the tensile strength of reinforcement before the bond to concrete fails. To this end, the bond stress is calculated using the nominal diameter of reinforcement and nominal anchorage length for sake of engineering approach, while in [2] the measured diameter was used instead. As the concrete strength varied between the pull-out series (see [2]), the concept of normalised bond strength is utilised [10] normalising the bond strength for the concrete cube compressive strength $f_{c,\,cube}$ = 56.3MPa, according to the formula:

$$\tau_b = \tau_b' \frac{\sqrt{f_{c,cube}}}{\sqrt{f_{c,cube}'}} \quad (1)$$

The tensile strength of reinforcement f_t is taken directly from [2], and presented together with the normalised maximum bond stress $\tau_{b,\,max}$ in Table 1. Those values are then used to calculate the theoretical anchorage length required to activate the full tensile strength of the reinforcement, including the standard deviations obtained in the experimental testing.

Table 1. *Values of tensile strength, maximum bond strength, and theoretical anchorage length to activate the complete tensile strength based on available results from [2].*

Reinforcement type	f_t [MPa]	$\tau_{b,\,max}$ [MPa]	$f'_{c,\,cube}$ [MPa]	$l_{b,rqd}$ [mm]	$l_{b,rqd}$ [Φ]
Commercial A 4 mm	613 ±25.3	13.4 ±2.4	59.3	46.5 ±14.7	11.6 ±3.7
Commercial A 6 mm	764 ±18.8	11.7 ±0.6	59.3	98.0 ±10.5	16.3 ±1.8
Commercial A 8 mm	793.1 ±24.8	16.8 ±0.1	59.3	94.4 ±5.0	11.8 ±0.6
Commercial B 4 mm	851.2 ±87.5	16.2 ±1.9	59.3	52.6 ±16.6	13.2 ±4.1
DWM 4mm 300 mA	788.1 ±81.8	16.6 ±0.8	56.3	47.3 ±10.2	11.8 ±2.6
DWM 6mm 300 mA	720.55 ±71.3	18.4 ±3.2	56.3	59.4 ±23.4	9.9 ±3.9

For comparison, in case of the standard steel hot-rolled reinforcement bars B500B with f_y = 500MPa and minimum R_m/R_e = *1.05*, the ultimate tensile strength is equal to f_t = *1.05 * 500MPa = 525MPa* [11]. Taking good conditions and diameter below 32 mm, and assuming concrete of class C45/55 based on the cube compressive strength of reference material, the minimum required anchorage is obtained as 15.3Φ. Of course, the designed anchorage length should consider appropriate partial safety factors, resulting in required length of around 28Φ. However, for sake of comparison with experimental results, the partial safety factors should not be considered.

This shows that: 1) reinforcement tested here requires similar anchorage length to the classical steel reinforcement, and 2) GFRP reinforcement produced with DWM presents similar properties to the commercially available prefabricated GFRP one.

3. Four-point bending testing

In order to verify the transferability of direct pull-out to the real structural behaviour, two series of testing under four-point bending (4P bending) are analysed. The testing procedure was inspired by methods applied for fibre reinforced cementitious composites [12], [13], where thin and wide plates are loaded in symmetrical four-point bending, see Figure 2. Subsequently, using proper modelling and principles of inverse analysis, the obtained force-deflection response can be translated to estimate material properties under tension. With certain modifications, this method can be used also for discrete continuous reinforcement, such are GFRP or steel reinforcement bars, as well as for large structural elements [8], [14].

3.1 Principles of inverse analysis

In order to conduct an inverse analysis, a simple spreadsheet-based computational model is established. The force-displacement datapoints from experimental testing are imported and translated to bending moment-deflection. For each datapoint, a classical formula (2) from elasticity theory is used to calculate the curvature φ based on: deflection δ, distance between supports L and distance between force application point and support a. Subsequently, the curvature is translated to strain at the bottom ε_b based on the position of the neutral axis $x_{(n\text{-}n)}$, see eq. (3).

$$\delta = \varphi / 24\,(3L^2 - 4a^2) \quad (2)$$

$$\varphi=\varepsilon_b / x_{(n\text{-}n)} \tag{3}$$

Since the position of neutral axis depends on the force balance in cross-section, it is taken at mid-heigh for the first data point, and then on basis of the calculation of neutral axis position of a previous datapoint for each subsequent datapoint. This is well-justified, as for the first datapoint the concrete is not cracked, and hence the stress distribution is as for a fully elastic material in this rectangular cross-section. Subsequently, the shift of the neutral axis position is stepwise as concrete cracking progresses, and therefore the calculation error is very small, provided that sufficient number of datapoints is taken into analysis.

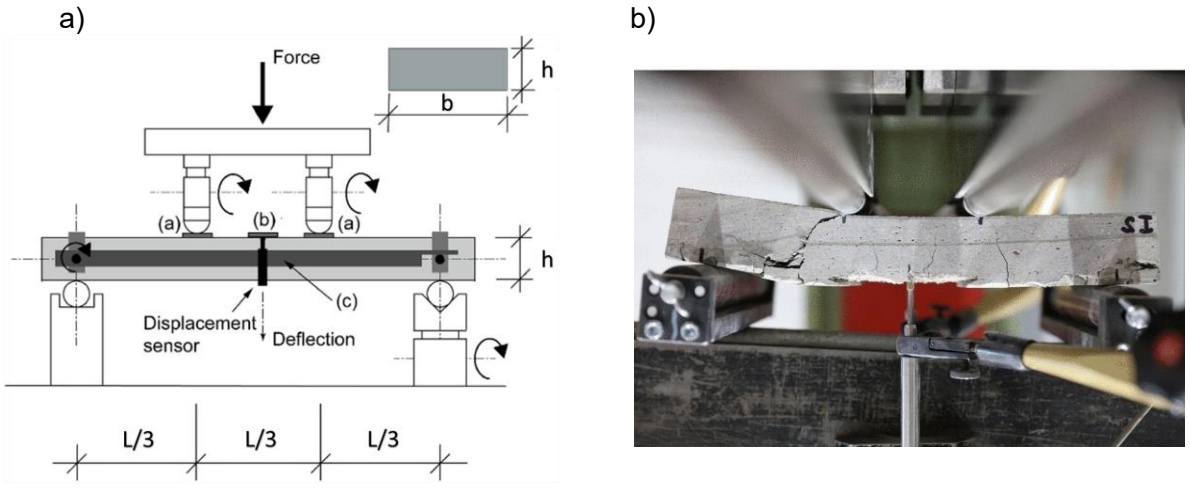

Figure 2. *a) Four-point bending testing setup and specimen shape for inverse analysis, adapted from [8]; b) Testing of sample with fibre wound reinforcement, adapted from [4].*

In order to calculate the internal stress distribution at each datapoint, a layered model is used under assumption of Euler- Bernoulli elastic beam theory and perfect bond. The cross-section is divided into 100 discrete layers representing concrete, and the additional layer representing reinforcement [14]. For a given ε_b, and respecting the defined constitutive stress-strain model for concrete and reinforcement, such a $x_{(n\text{-}n)}$ is found that the sum of forces is equal to zero. Subsequently, the resulting mending moment M_{cal} is calculated.

As such, for each datapoint and resulting ε_b and $x_{(n\text{-}n)}$, a M_{cal} is obtained, reflecting the assumed material properties. The resulting deflection, calculated again with formulas (2) and (3), is almost identical to measured one, with the discrepancy stemming from the previously utilised procedure to translate experimental results to ε_b; this discrepancy is confirmed to be minimal. If needed, the calculation can be re-run, updating the approximations of $x_{(n\text{-}n)}$. As such, the theoretical bending moment-deflection curve is obtained.

In the procedure of inverse analysis such material properties are found, that the calculated and experimental bending moment-deflection curve are similar. The input material properties are then representative for the real as-build material properties, respecting the simplifications used in the procedure. This approach is established for fibre-reinforced cementitious materials. It was also experimentally confirmed for large elements with discrete reinforcement through strain measurement and comparison with the theoretically obtained strain distribution [8].

Due to relatively large scatter of obtained results, the inverse analysis is performed simultaneously for all specimens from a given testing series, rather than one by one for each specimen. Furthermore, the theoretical [7] or mean [4] thickness of specimens is taken respectively. As such, the obtained fitted values should be treated as an approximative one.

The above procedure is valid for small deformations, i.e., without formation of plastic hinge in the critical crack cross-section of the tested element, as well as for perfect bond of reinforcement. Once those assumptions are no more valid, the modelled curve ceases to follow the experimental one. As the GFRP exhibits no plastic deformation, the formation of plastic hinge could result only from crushing of concrete, which can be verified during the inverse analysis. Therefore, the divergence of theoretical and experimental curves will most certainly indicate the onset of pull-out failure, and as such will be used to verify whether the previously calculated required anchorage length holds in the tested specimens.

In the same time, the calculated reinforcement stress could not be used to estimate the bond stress, as to this end the location of critical crack defining the anchorage length should be precisely measured. This information is not included in the databases.

3.2 Material models and properties

In all experimental campaigns the same cementitious material was used, Nafufill KM 250, with maximum aggregate size 2mm. The producer declares 28 days compressive modulus of elasticity $E_{c,\,cast}$ = 22.6 GPa and $E_{c,\,spray}$ = 26.0 GPa, while the compressive strength $f_{c,\,cast}$ = 55 MPa and $f_{c,\,spray}$ = 68.1 MPa, respectively for cast and for sprayed material application process [15]. Own previous research consistently shown however the mean compressive strength around $f_{c,\,spray}$ = 80MPa, and this value is used for sprayed concrete, while per proportionality value $f_{c,\,cast}$ = 65MPa is used for cast concrete, due to lack of assisting material testing specimens. There is no information available regarding the direct tensile material properties, and they are fitted based on the experimental results within realistic range.

For cementitious material in compression, a bi-linear perfectly elastic-perfectly plastic material model was taken. The end of plastic plateau is assumed at $\varepsilon_{cu3} = 1.2\,\varepsilon_{c3}$, where the latter is the end of elastic state as defined by f_c and E_c; a similar ratio is expected in material of such compressive strength [11]. For cementitious material in tension, a perfectly elastic-softening model was taken, despite the fact that similar materials are better characterised by a bi-linear softening behaviour [16]. For sake of simplification, the third branch was disregarded, with the second branch ending at the inflection point, i.e. at point $f_{ct,soft}$, $\varepsilon_{ct,\,soft}$. Due to lack of reliable information on the used material, realistic values were fitted on basis of experiments. They were supported by the results of 3 point bending testing of the accompanying 7 x 7 x 28 cm^3 specimens available with one of datasets presented here [7], consistently showing the ultimate tensile strength f_{ct} in the range of around 3.5 MPa; they are not discussed here for sake of brevity. No information regarding the descending branch is available, however due to presence of synthetic fibres it is expected that the fracture energy is relatively large.

For GFRP, a linear perfectly elastic model is adopted until tensile failure, representing well the behaviour of this material in direct tension. Both material properties, i.e., modulus of elasticity E_{GFRP} and tensile strength f_{GFRP} are fitted in the inverse analysis procedure.

3.3 Influence of transverse reinforcement and material deposition method

The first dataset is for frame-winding reinforcement with two layouts of transverse reinforcement, and with two concrete application methods: cast concrete and digitally sprayed concrete using Shotcrete 3D Printing (SC3DP) [7]. After deposition of the first layer of concrete, the frame with wound reinforcement is placed directly on the fresh concrete, and subsequently the remaining concrete applied. After hardening, the top surface is CNC-milled, and an element cut into six identical plates. For each combination of transverse reinforcement and concrete application, six plates were tested under span L=300 mm, each one with dimensions: length = 400 mm x b = 150 mm x h = 55 mm, with reinforcement depth of 11 mm, see Figure 3.

The 19200 tex e-glass direct roving is used as primary fibre strand resulting in the reinforcement diameter of approx. 4 mm. The secondary fibre EC-9 136 X3 S135 is wound helically with a pitch of 7 mm and pre-tensioned by a hysteresis break set to 150 mA, resulting in a resistance torque of approx. 24 N/mm. A Carboplast resin L 285 and hardener H 286 epoxy resin is used. This reinforcement can be compared to previously discussed 'DWM 4mm 300 mA' reinforcement due to the same primary strand, but with smaller hysteresis break (150 mA vs 300 mA) and a larger secondary yarn pitch (7 mm vs 4 mm). In all cases five longitudinal strands were present in each specimen, while the number and distribution of the transverse strands varied, see Figure 3.

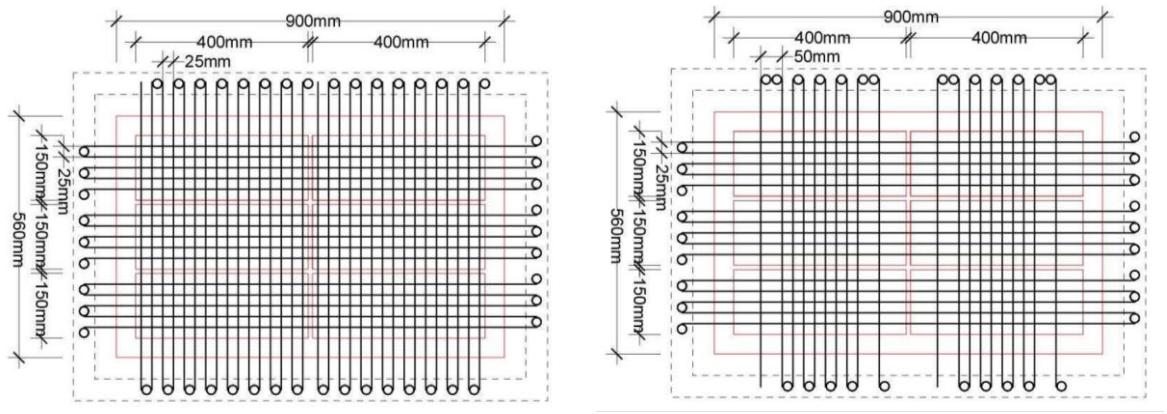

***Figure 3**. Two layouts of transverse reinforcement in fabricated elements; from each six identical specimens were extracted and tested; adapted from [7].*

***Table 2.** Fitted material properties for specimens with variable transverse reinforcement.*

Test series	$f_{c,t}$ [Mpa]	$f_{softening}$ [Mpa]	f_{GFRP} [Mpa]	E_{GFRP} [Gpa]
Cast, Reinforcement A	2.3	1.2	550	41
Cast, Reinforcement B	2.3	1.2	550	40
SC3DP, Reinforcement A	2.3	1.2	720	35
SC3DP, Reinforcement B	2.3	1.2	850	38

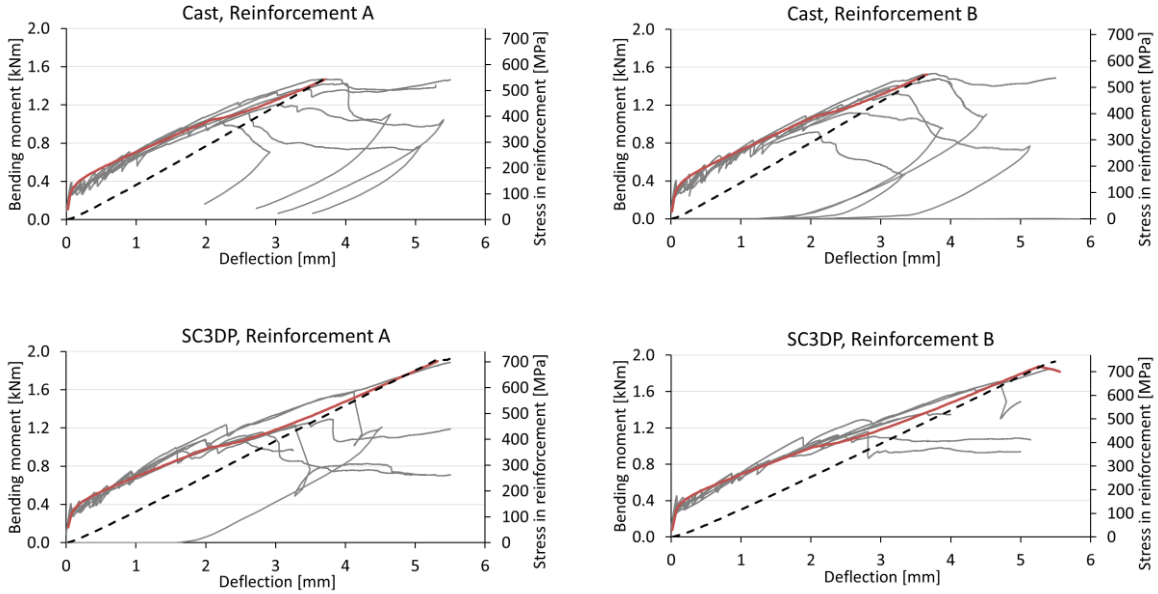

Figure 4. *Experimental and fitted bending moment - deflection curves for specimens with variable transverse reinforcement, with calculated stress in reinforcement; bending moment - deflection curves measured (gray) and fitted (red) and calculated reinforcement stress (black dashed).*

The fitted material properties are presented in Table 2, while the fitted curves are presented in Figure 4. The range of y-axis for stress in reinforcement was proportionally aligned to the obtained bending moment-deflection curve, i.e., the achieved stress for a given bending moment can be directly taken from the figure.

It is clear that in any case a relatively large scatter was achieved. For example, for cast specimens with reinforcement type A, one of specimens failed under bending moment of around 1.1 kNm resulting in stress in reinforcement of around 400 MPa, while for other specimen the failure occurred at around 1.5 kNm, hence stress of around 550 MPa. This can be observed for all testing series. No clear difference was exhibited for two arrangements of the transverse reinforcement.

The cast specimens are coherently weaker than the sprayed specimens, proving the importance of well controlled cementitious material deposition, as well as difference in hardened properties depending on the deposition method. In case of some of the sprayed specimens, the model exhibited failure of concrete in compression. In reality, it could be either this mode of failure, or failure of reinforcement in tension, as the achieved stress is close to the lower bound of direct tensile results and both modes lead to sudden collapse. The dataset does not contain any observations which could indicate the mode of failure.

On basis of previously mentioned similarities to ‘DWM 4mm 300 mA’ (compare Table 1) it can be stated that most of the achieved results are well below the true tensile strength, and the premature failure in all cases stems from weaker bond, probably due to the lower hysteresis break and larger pitch. It would also indicate that the specimen cross-section was in fact over-reinforced, but failing in tension due to somewhat weaker tensile bond.

3.4 Built-in vs reference specimens

Another dataset [4] investigated fibre winding supporting shotcrete. In order to improve the concrete deposition process, a glass fibre fleece tape was automatically deposited with the last layer of GFRP reinforcement. It formed a thin, complex-curved surface onto which concrete was sprayed. After the exposition of the demonstrator, in total twelve plates were sawn-cut from it: six from the lower and six from the upper part of the executed structure, to investigate the influence of respectively inclined and almost horizontal surface orientation during concrete deposition. Subsequently, at thin concrete layer was sprayed on the surface of exposed reinforcement at the back surface of the demonstrator.

Additionally, reference reinforced specimens with and without the fleece tape were prepared, four of each type, to investigate its influence on the bond. They were prepared similarly to the ones described before, i.e., the layer of concrete was sprayed, subsequently the reinforcement installed, and the SC3DP continued until the full height was achieved.

In this case thinner, 9600 tex e-glass fibre roving was chosen, resulting in 3 mm diameter. That thin fibre rowing was not tested in the previously mentioned experiments. The secondary helical fibre was the same as previously, i.e., EC-9 136 X3 S135 with pitch 7mm. All plates had dimension 300 mm x 120 mm, thickness around 40mm (see [4]), and testing span of 255 mm. The results are presented in Table 3 and Figure 5.

Again, large scatter in each series can be noticed. Importantly, due to different geometry of the specimens, a similar bending moment is achieved for reference and demonstrator specimens, while the achieved reinforcement stress in reference specimens is higher. Likewise, despite apparently less stiff response of the reference specimens, the fitted E_{GFRP} are higher for reference series than for the demonstrator, reflecting potentially better bond mechanism in reference specimens, as well as a slight slip due to the presence of the tape.

The fitted f_{GFRP} is quite smaller in the demonstrator than in the reference specimens indicating lower bond strength, probably as the concrete was first applied only from one side of the reinforcement, and only later applied from the other. Thus, it did not penetrate and embedded the reinforcement and the fleece tape. Furthermore, a delamination of the old and new concrete at the level of the fleece tape could have been observed towards the end of the specimen testing, as visible towards the left support on the Figure 2 b).

Interestingly, the $f_{c,t}$ fitted for reference specimens was significantly lower than for other specimens, which cannot be explained on basis of the available data.

Table 3. *Fitted material properties for specimens from demonstrator and assisting ones.*

Test series	$f_{c,t}$ [Mpa]	$f_{softening}$ [Mpa]	f_{GFRP} [Mpa]	E_{GFRP} [Gpa]
Demonstrator, Bottom	2.3	1.2	570	18
Demonstrator, Top	2.3	1.2	530	16
Reference, w. tape	1.8	0.5	700	20
Reference, w/o tape	1.8	1.2	780	24

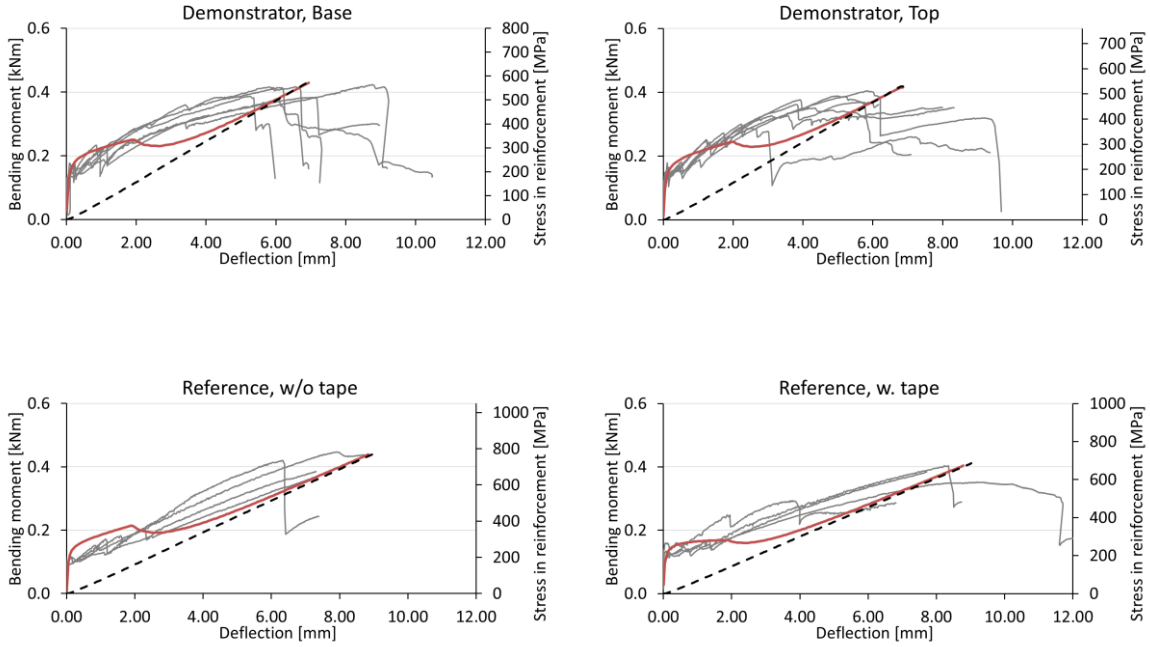

***Figure 5**. Experimental and fitted bending moment - deflection curves for specimens from demonstrator and assisting ones, with calculated stress in reinforcement; bending moment - deflection curves measured (gray) and fitted (red), and calculated reinforcement stress (dashed black).*

4. Discussion

As presented in the above experimental research, the understanding of structural behaviour of in-situ fabricated GFRP reinforcement is crucial, and non-trivial. It stems from the number of parameters influencing the required anchorage length, and is conjoint with the quality of resin penetration, as discussed already in [2]. Furthermore, multiple modes of bond failure can be expected, including the failure of the secondary yarn of the reinforcement through rupture or debonding from the primary yarn. As such, further investigation of those parameters is crucial to indicate the best set of fabrication parameters resulting in the optimised design of the reinforcement strand. Such an optimised strand can be later implemented in the reinforced concrete element with foreseeable structural properties.

The used concrete material and deposition method is of critical importance, as well. Furthermore, to correctly analyse the obtained testing data, the accompanying specimens are required, providing information on its compressive and tensile properties. This requires interdisciplinarity encompassing material, structural, and civil engineers collaborating with the architects, as well as meticulous planning and execution. Last but not least, the design of specimens needs to be carefully considered to reflect the intended application method.

As demonstrated, on basis of the pull-out testing it can be stated that the anchorage length of around 60 mm is sufficient to activate the full tensile strength of 4 mm reinforcement even in cast concrete. However, when the similar reinforcement was tested under bending in the section 3.3 it failed largely below its tensile strength through pull-out, indicating too short anchorage length, although it was longer than theoretically required 60 mm. The above demonstrates the complexity which comes with the freedom of fabrication.

5. Conclusions

This paper discusses performance of wound GFRP reinforcement from perspective of the required anchorage length on basis of available datasets, i.e., one dataset presenting the direct pull-out testing from unconfined concrete cube, and two datasets presenting four-point bending of reinforced concrete plates. Those datasets where not analysed before up to this level of detail. On this basis, the following remarks can be drawn:

- Under favourable conditions, and with appropriate reinforcement fabrication settings (hysteresis break, secondary yarn pitch), the in-situ wound reinforcement can have similar required anchorage length as classical steel reinforcement bars.
- The analysis of reinforced concrete plates proven, that the reinforcement fails through pull-out, despite anchorage much longer than theoretically required; additional research is needed to indicate the reasons for that
- When the same cementitious material is applied in two manners (cast vs sprayed), the resulting bond with the identical reinforcement can be radically different.

All the above demonstrates, that while the digital fabrication enables freedom, it causes multiple parameters to interact. Thus, carefully planned, holistic, and interdisciplinary research is required to further advance the knowledge, and clearly identify which parameters or details need be corrected for successful implementation of digital methods into practice.

Data availability statement

Raw data was provided by the authors of publications [2], [4], [7], in particular by Tom Rothe and Stefan Gantner. Their willingness to sort, provide, and explain the data and the testing procedures is kindly acknowledged. No new data was produced.

Author contributions

B.S.: Conceptualization, Data curation, Formal analysis, Investigation, Methodology, Resources, Software, Validation, Visualization, Writing – original draft. N.H. and H.K.: Funding acquisition, Project Administration, Writing – review & editing.

Competing interests

The authors declare that they have no competing interests.

Funding

This research was partially funded by the DFG Collaborative Research Centre TRR 277 AMC (Additive Manufacturing in Construction, 414265976), subproject A05: Integration of Individualized Prefabricated Fibre Reinforcement in Additive Manufacturing with Concrete.

References

[1] T. Rothe, S. Gantner, N. Hack, and C. Hühne, ‘A Dynamic Winding Process of Individualized Fibre Reinforcement Structures for Additive Manufacturing in Construction’, *Open Conference Proceedings*, vol. 3, Dec. 2023, doi: 10.52825/ocp.v3i.187.

[2] T. Rothe, J. Pösch, S. Gantner, N. Hack, and C. Hühne, ‘Optimization of tensile properties and bond behaviour to concrete of fibre reinforcement strands produced within a dynamic

fibre winding process', presented at the 11th International Conference on FPR Composites in Civil Engineering, Rio de Janeiro, Brasil, 2023.
[3] H. Kloft *et al.*, 'Interaction of reinforcement, process, and form in Digital Fabrication with Concrete', *Cement and Concrete Research*, vol. 186, p. 107640, Dec. 2024, doi: 10.1016/j.cemconres.2024.107640.
[4] S. Gantner *et al.*, 'Robotic frame winding: prefabricated fibre structures as formwork and reinforcement for digitally fabricated shell-like concrete elements', *Constr Robot*, vol. 9, no. 1, p. 12, May 2025, doi: 10.1007/s41693-025-00154-0.
[5] S. Gantner, P. Rennen, T. Rothe, C. Hühne, and N. Hack, 'Core Winding: Force-Flow Oriented Fibre Reinforcement in Additive Manufacturing with Concrete', in *Third RILEM International Conference on Concrete and Digital Fabrication*, R. Buswell, A. Blanco, S. Cavalaro, and P. Kinnell, Eds., Cham: Springer International Publishing, 2022, pp. 391–396. doi: 10.1007/978-3-031-06116-5_58.
[6] P. Rennen *et al.*, 'Robotic knitcrete: computational design and fabrication of a pedestrian bridge using robotic shotcrete on a 3D-Knitted formwork', *Front. Built Environ.*, vol. 9, Dec. 2023, doi: 10.3389/fbuil.2023.1269000.
[7] P. Rennen *et al.*, 'Structural Evaluation of Shotcrete 3D Printing and Robotic Fiber Winding for Thin Shell Elements', 2024.
[8] B. Sawicki, E. Brühwiler, and E. Denarié, 'Inverse Analysis of R-UHPFRC Beams to Determine the Flexural Response under Service Loading and at Ultimate Resistance', *J. Struct. Eng.*, vol. 148, no. 2, p. 04021260, Feb. 2022, doi: 10.1061/(ASCE)ST.1943-541X.0003239.
[9] RILEM RC6, *RC 6 Bond test for reinforcement steel. 2. Pull-out test*, 1983. Accessed: Jun. 24, 2025. [Online]. Available: https:///https://www.rilem.net/publication/publication/4?id_papier=4020
[10] P. R. Shunmuga Vembu and A. K. Ammasi, 'A Comprehensive Review on the Factors Affecting Bond Strength in Concrete', *Buildings*, vol. 13, no. 3, Art. no. 3, Mar. 2023, doi: 10.3390/buildings13030577.
[11] EC2, *Eurocode 2: Design of concrete structures-Part 1-1: General rules and rules for buildings*, EN 1992-1-1, 2005.
[12] SIA 2052, 'Technical Leaflet SIA 2052, UHPFRC - Materials, design and construction, Swiss Society of Engineers and Architects, Zurich'. Swiss Society of Engineers and Architects, Zurich, 2017.
[13] AFGC, *Ultra High Performance Fibre-Reinforced Concretes, Recommendations, Revised edition, June 2013*. in Documents scientifiques et techniques (édition AFGC). Association Francaise de Genie Civil, 2013. Accessed: Jun. 17, 2020. [Online]. Available: https://www.afgc.asso.fr/app/uploads/2007/10/Recommandations-BFUP-Juin-2013.pdf
[14] B. Sawicki and E. Brühwiler, 'Experimental and Analytical Investigation of Deflection of R-UHPFRC Beams Subjected to Loading–Unloading', *International Journal of Concrete Structures and Materials*, vol. 18, no. 1, p. 6, Jan. 2024, doi: 10.1186/s40069-023-00636-x.
[15] MC Bauchemie, 'Nafufill KM 250 Technical Datasheet'. MC-Bauchemie Müller GmbH & Co. KG, Jun. 2025. Accessed: Jul. 18, 2025. [Online]. Available: https://pim.mc-bauchemie.de/media/MCBAUCHEMIEData/DO/base/Nafufill_KM_250_DE_DE_EN_TDS.pdf
[16] J. Huang and V. C. Li, 'A meso-mechanical model of the tensile behaviour of concrete. part II: modelling of post-peak tension softening behaviour', *Composites*, vol. 20, no. 4, pp. 370–378, Jul. 1989, doi: 10.1016/0010-4361(89)90662-9.